



MODELING SOLUTE REDISTRIBUTION AND MICROSTRUCTURAL DEVELOPMENT IN FUSION WELDS OF Nb-BEARING SUPERALLOYS

J. N. DUPONT¹†, C. V. ROBINO² and A. R. MARDER¹

¹Department of Materials Science and Engineering, Lehigh University, Bethlehem, PA 18015-3195, U.S.A. and ²Sandia National Laboratories, Albuquerque, NM, U.S.A.

(Received 9 March 1998; accepted 19 March 1998)

Abstract—Solute redistribution and microstructural evolution have been modeled for gas tungsten arc fusion welds in experimental Ni base and Fe base Nb-bearing superalloys. The multi-component alloys were modeled as a ternary system by grouping the matrix (Fe, Ni, Cr) elements together as the “solvent” to form the γ component of the γ -Nb-C “ternary system”. The variation in fraction liquid and liquid composition during the primary $L \rightarrow \gamma$ and eutectic type $L \rightarrow (\gamma + \text{NbC})$ stages of solidification were calculated for conditions of negligible Nb diffusion and infinitely fast C diffusion in the solid phase. The proposed model is based on modifications of solute redistribution equations originally developed by Mehrabian and Flemings. Results of the calculations were superimposed on the pseudo-ternary γ -Nb-C solidification surfaces to predict the solidification reaction sequences along with the total and individual amounts of γ/NbC and γ/Laves eutectic-type constituents which form during solidification. Comparison was made to experimentally measured values, and reasonable agreement was found. The model results permit quantitative interpretations of composition–microstructure relations in these Nb-bearing experimental alloys and should provide useful insight into comparable commercial alloy systems as well. © 1998 Acta Metallurgica Inc. Published by Elsevier Science Ltd. All rights reserved.

NOMENCLATURE

| | |
|------------|---|
| C_e | eutectic composition |
| C_l | liquid composition |
| C_o | nominal composition |
| C_s | solid composition |
| f_e | fraction of eutectic |
| f_l | fraction of liquid |
| f_s | fraction of solid |
| f_γ | fraction of primary γ |
| k_{ij} | equilibrium distribution coefficient for element j between phase i and the liquid |

1. INTRODUCTION

Ni base and Fe base Nb-strengthened alloys represent a significant portion of superalloys currently in use. Commercial examples include alloys IN625 [1], IN718 [2], IN903 [3], IN909 [4], and Thermo-Span [5], to name a few. These alloys are often used for components which are fabricated by solidification processes such as casting and fusion welding. Previous studies conducted on these commercial superalloys have shown that minor additions of Nb and C strongly affect the type and amount of secondary phases which form during the terminal stages of solidification. In particular, two types of secondary phases, NbC and Laves, are known to form. Although several detailed investi-

gations have been conducted on specific commercial alloy systems, no general model has been developed to quantitatively predict microstructural evolution during solidification.

In previous articles [6, 7], solidification reaction sequences, equilibrium distribution coefficients, and γ -Nb-C “pseudo-ternary solidification surfaces” were described for a wide range of experimental Fe base and Ni base Nb-bearing superalloys which simulate typical composition variations encountered in commercial systems. The experimental alloys utilized in that work initiated primary solidification according to $L \rightarrow \gamma$, which enriched the interdendritic liquid in Nb and C until the eutectic-type $L \rightarrow (\gamma + \text{NbC})$ reaction occurred. The alloys generally terminated solidification by a second eutectic-type reaction, $L \rightarrow (\gamma + \text{Laves})$. This solidification reaction sequence is similar to that expected in the ternary Ni–Nb–C system. Based on this similarity, the multi-component alloys were modeled as a ternary system by grouping the matrix (Fe, Ni, Cr) elements together as the “solvent” to form the γ component of the γ -Nb-C pseudo-ternary solidification diagram. This so-called pseudo-ternary solidification diagram is analogous to a liquidus surface of a true ternary system. The locations of the lines of twofold saturation separating the γ , NbC, and Laves primary phase fields on the solidification diagram were determined using microstructural characterization techniques. Since the segregation

†To whom all correspondence should be addressed.

potential of Nb was found to depend on the nominal iron content of the alloy, two separate diagrams were developed; one for the Ni base alloys and one for the Fe base alloys. In addition, the Scheil equation and equilibrium lever law were shown to provide reasonably accurate descriptions of solute redistribution for Nb and C, respectively. This result is useful as it avoids the need for considering detailed kinetic effects associated with diffusion of solute in the solid and permits development of a relatively simple analytical treatment of solute redistribution during solidification. In this article, the experimentally determined equilibrium distribution coefficients and pseudo-ternary solidification surfaces are applied to develop a solidification model which describes solute redistribution and associated microstructural development. The model is based on a previous approach proposed by Mehrabian and Flemings [8] which assumes negligible solid state diffusion of each solute in a ternary system. Their model is modified to account for infinitely fast diffusion of C and applied to the pseudo-ternary approach utilized here. Results of the total and individual amounts of eutectic type constituents calculated with the model are compared to the measured values, and reasonable agreement is found. The modeling results provide the framework for detailed interpretations of composition–solidification microstructure relations in fusion welds of Nb-bearing superalloys.

2. EXPERIMENTAL PROCEDURE

The experimental procedures have been described elsewhere [6, 7] and detail will not be repeated here. The experimental alloy compositions are summarized in Table 1. The alloys contain factorial vari-

ations in Fe (in exchange for Ni), Nb, Si, and C at two levels. Several additional alloys with intermediate C contents (Alloys 1.5, 3.5, 7.5, and 11.5) were also investigated. Autogenous welds on these specimens were prepared using the gas tungsten arc (GTA) process at a current of 95 A, 2.5 mm arc gap (10 V), and 3.3 mm/s travel speed. Two high Nb alloys (Ni – 1 and Fe – 1) were also added to produce alloys with high quantities of eutectic-type constituents. Scanning Electron Microscopy was conducted on the weld metals using a JEOL 6300 Field Emission Gun Scanning Electron Microscope (FEG-SEM) at an accelerating voltage of 15 kV. Quantitative Image Analysis (QIA) was conducted on at least ten SEM photomicrographs from each weld. Area fractions of total eutectic type contents and, where possible, individual γ /NbC and γ /Laves eutectic-type constituents were measured along the centerline of each weld with at least ten SEM photomicrographs. Area fractions were assumed to be equivalent to volume fractions. Phase identification of the NbC and Laves phases was accomplished by a combination of electron microprobe microanalysis and backscattered electron kikuchi patterns and is discussed elsewhere [6, 7].

3. MODELING SOLUTE REDISTRIBUTION

3.1. Negligible diffusion of each solute (Mehrabian–Flemings model)

The Mehrabian–Flemings (M–F) model [8] is briefly outlined here in relation to the solidification behavior of the Nb-bearing alloys of interest to this study since it forms the basis for the appropriate modification needed to account for the high diffusivity of C in austenite. The M–F model is based upon the same assumptions used in the Scheil

Table 1. Alloy compositions. All values in wt%

| Alloy | Fe | Ni | Cr | Nb | Si | C | P | S |
|--------|-------|-------|-------|-------|------|-------|-------|-------|
| 1 | 10.49 | 68.53 | 18.90 | 1.93 | 0.08 | 0.017 | 0.004 | 0.003 |
| 1.5 | 10.75 | 67.95 | 19.21 | 2.00 | 0.03 | 0.052 | 0.004 | 0.003 |
| 2 | 11.12 | 68.20 | 19.12 | 1.95 | 0.06 | 0.132 | 0.004 | 0.002 |
| 3 | 10.70 | 68.11 | 19.02 | 1.82 | 0.38 | 0.010 | 0.004 | 0.003 |
| 3.5 | 10.39 | 66.80 | 19.29 | 1.94 | 0.41 | 0.075 | 0.004 | 0.003 |
| 4 | 10.72 | 67.60 | 19.08 | 1.91 | 0.40 | 0.155 | 0.004 | 0.001 |
| 5 | 10.84 | 65.79 | 18.98 | 5.17 | 0.05 | 0.013 | 0.005 | 0.010 |
| 6 | 10.88 | 65.22 | 18.89 | 4.87 | 0.08 | 0.161 | 0.005 | 0.007 |
| 7 | 10.70 | 65.53 | 19.30 | 4.86 | 0.52 | 0.010 | 0.005 | 0.009 |
| 7.5 | 10.82 | 63.93 | 18.54 | 4.92 | 0.46 | 0.081 | 0.005 | 0.004 |
| 8 | 10.80 | 64.96 | 18.90 | 4.72 | 0.52 | 0.170 | 0.005 | 0.007 |
| Ni – 1 | 7.71 | 55.03 | 18.23 | 17.79 | 1.03 | 0.08 | ND | ND |
| 9 | 46.03 | 33.56 | 19.31 | 1.66 | 0.10 | 0.003 | 0.006 | 0.003 |
| 10 | 46.69 | 32.80 | 19.70 | 1.66 | 0.01 | 0.108 | 0.006 | 0.002 |
| 11 | 45.38 | 32.80 | 19.53 | 1.77 | 0.57 | 0.004 | 0.006 | 0.002 |
| 11.5 | 47.38 | 31.05 | 19.64 | 1.84 | 0.67 | 0.116 | 0.006 | 0.001 |
| 12 | 45.28 | 32.39 | 19.89 | 1.93 | 0.61 | 0.079 | 0.006 | 0.002 |
| 13 | 44.55 | 31.24 | 19.63 | 4.42 | 0.02 | 0.015 | 0.007 | 0.003 |
| 14 | 44.05 | 31.93 | 19.52 | 4.51 | 0.08 | 0.210 | 0.006 | 0.002 |
| 15 | 45.40 | 30.03 | 19.54 | 4.88 | 0.66 | 0.010 | 0.007 | 0.003 |
| 16 | 44.47 | 30.89 | 19.45 | 4.77 | 0.64 | 0.216 | 0.006 | 0.002 |
| Fe – 1 | 40.87 | 27.89 | 19.69 | 10.63 | 0.63 | 0.081 | ND | ND |

ND, not determined.

equation: dendrite tip undercooling and solid state diffusion (of each solute) are negligible, thermodynamic equilibrium is maintained at the solid/liquid interface, and diffusion is infinitely fast in the liquid. The treatment contains two sets of solute redistribution relations. The first set describes the variation in liquid composition during solidification of the primary phase, while the second set describes solute redistribution during eutectic-type reactions which occur along the line of twofold saturation.

The relation describing the variation in liquid composition during solidification of the primary phase (using Nb and C as the “solute” elements) is given as [8]

$$C_{l,Nb} = C_{o,Nb} \left(\frac{C_{l,C}}{C_{o,C}} \right)^{(k_{Nb}-1)/(k_C-1)} \quad (1)$$

The symbols are defined in the Nomenclature. When the liquid composition given by equation (1) intersects a line of twofold saturation on the liquidus surface, the remaining fraction liquid (f_l) will transform to one or more eutectic-type constituents. Thus, the value of f_l at that point represents the total amount of eutectic-type constituents (γ/NbC plus $\gamma/Laves$) in the final microstructure. In order to calculate the total volume fraction of eutectic-type constituent, f_e , the line of twofold saturation on the liquidus surface is first represented by a linear equation

$$C_{l,C} = a + bC_{l,Nb} \quad (2)$$

Solving equation (2) in terms of $C_{l,Nb}$ and setting equal to equation (1) yields the carbon content in the liquid, $C_{l,C}$, at the intersection point

$$\frac{C_{l,C} - a}{b} = C_{o,Nb} \left(\frac{C_{l,C}}{C_{o,C}} \right)^{(k_{Nb}-1)/(k_C-1)} \quad (3)$$

The corresponding Nb content in the liquid is given by substituting this value of $C_{l,C}$ into either equation (1) or equation (2). The value of $C_{l,Nb}$ at this point can be taken as the value of $C_{e,Nb}$ (the “eutectic” composition) in the Scheil equation to calculate the amount of total eutectic-type constituent in the as-solidified microstructure

$$f_e = \left(\frac{C_{e,Nb}}{C_{o,Nb}} \right)^{1/(k_{Nb}-1)} \quad (4)$$

When the primary solidification path intersects the line of twofold saturation separating the γ and NbC phases, the solidification reaction changes from $L \rightarrow \gamma$ to $L \rightarrow (\gamma + NbC)$ as the two solid phases begin forming from the liquid. In this case, the mass balance for Nb is given by [8]

$$df_\gamma(C_{l,Nb} - C_{\gamma,Nb}) + df_{NbC}(C_{l,Nb} - C_{NbC,Nb}) = f_l dC_{l,Nb} \quad (5)$$

where $C_{i,j}$ is the concentration of element j in phase i . Writing an overall differential mass balance

$$df_\gamma = -df_{NbC} - df_l \quad (6)$$

and expressing the solid compositions $C_{\gamma,Nb}$ and $C_{NbC,Nb}$ in terms of liquid composition through the distribution coefficient

$$C_{\gamma,Nb} = k_{\gamma,Nb} C_{l,Nb} \quad (7a)$$

$$C_{NbC,Nb} = k_{NbC,Nb} C_{l,Nb} \quad (7b)$$

where $k_{i,j}$ is the distribution coefficient for element j between phase i and the liquid.

Inserting equations (6), (7a) and (7b) into equation (5) and rearranging yields

$$\frac{df_l}{dC_{l,Nb}} = -\frac{1}{(1-k_{\gamma,Nb})C_{l,Nb}} - \frac{(k_{NbC,Nb} - k_{\gamma,Nb})}{(1-k_{\gamma,Nb})} \frac{df_{NbC}}{dC_{l,Nb}} \quad (8a)$$

Since NbC is a stoichiometric phase, the value of $C_{NbC,Nb}$ can be considered constant and $k_{NbC,Nb}$ can therefore be determined through equation (7b) when $C_{l,Nb}$ is known. Thus, at any particular value of $C_{l,Nb}$ along the line of twofold saturation, all the values except f_l and $df_{NbC}/dC_{l,Nb}$ in equation (8a) are known. An expression for $df_{NbC}/dC_{l,Nb}$ can be obtained by first applying the same mass balance procedure described above for C. The result is analogous to equation (8a)

$$\frac{df_l}{dC_{l,C}} = -\frac{1}{(1-k_{\gamma,C})C_{l,C}} - \frac{(k_{NbC,C} - k_{\gamma,C})}{(1-k_{\gamma,C})} \frac{df_{NbC}}{dC_{l,C}} \quad (8b)$$

The carbon and niobium concentrations in the liquid along the line of twofold saturation are related by equation (2)

$$dC_{l,C} = b dC_{l,Nb} \quad (9)$$

Inserting equation (9) into equation (8b), solving for $df_{NbC}/dC_{l,Nb}$

$$\frac{df_{NbC}}{dC_{l,Nb}} = -\frac{df_l}{dC_{l,Nb}} \frac{(1-k_{\gamma,C})}{(k_{NbC,C} - k_{\gamma,C})} - \frac{b}{(k_{NbC,C} - k_{\gamma,C})} \frac{f_l}{C_{l,C}} \quad (10)$$

and inserting equation (10) into equation (8a) provides a relation between $df_l/dC_{l,Nb}$, f_l , $C_{l,Nb}$ and $C_{l,C}$

$$\frac{df_l}{dC_{l,Nb}} = \frac{f_l}{(1-k_{\gamma,Nb})} \left[\frac{b}{C_{l,C}} \frac{(k_{NbC,Nb} - k_{\gamma,Nb})}{(k_{NbC,C} - k_{\gamma,C})} - \frac{1}{C_{l,Nb}} \right] \left[1 - \frac{(1-k_{\gamma,C})}{(1-k_{\gamma,Nb})} \frac{(k_{NbC,Nb} - k_{\gamma,Nb})}{(k_{NbC,C} - k_{\gamma,C})} \right] \quad (11)$$

The distribution coefficients for Nb and C in γ are assumed to be constant at the values measured previously [1,7]. The concentration of C in NbC found in Ni-16Cr-8Fe alloys has been reported as 9.5 wt% C [9]. Therefore, the values of $C_{NbC,Nb}$ and $C_{NbC,C}$ are taken as 90.5 wt% Nb and 9.5 wt% C, respectively. This is in agreement with the

EPMA data reported in the previous article [6]. Equation (11) describes the variation in fraction liquid with liquid composition ($C_{1,Nb}$ and $C_{1,C}$) at any value of f_l along the line of twofold saturation between γ and NbC. This relation can be used to calculate solute redistribution during the eutectic-type $L \rightarrow (\gamma + NbC)$ reaction using an iterative scheme. The first value of $f_l (=f_e)$, $C_{1,Nb}$ and $C_{1,C}$ are calculated from the intersection of the solidification path and line of twofold saturation, as given by equations (2)–(4). These values are used to calculate the first value of $(df_l/dC_{1,Nb})_1$. The value of $(C_{1,Nb})_1$ is then incremented by a very small amount, $\Delta C_{1,Nb}$, along the line of twofold saturation to a new value of $(C_{1,Nb})_2 = (C_{1,Nb})_1 + \Delta C_{1,Nb}$. The corresponding value of $(C_{1,C})_2$ is determined through equation (2). The corresponding value of $(f_l)_2$ is calculated by

$$(f_l)_2 = (f_l)_1 + \left(\frac{df_l}{dC_{1,Nb}} \right)_1 \Delta C_{1,Nb}. \quad (12)$$

The values of $k_{NbC,Nb}$ and $k_{NbC,C}$ are calculated at each step by knowledge of the NbC and liquid compositions. When the values of $C_{1,Nb}$ and $C_{1,C}$ reach the class II reaction where the $L \rightarrow (\gamma + NbC)$ transformation is replaced by the $L \rightarrow (\gamma + \text{Laves})$ transformation [6, 7], the remaining fraction liquid at that point transforms to the γ/Laves eutectic-type constituent and solidification is complete.

The procedure above provides the relation between the fraction liquid and liquid composition at any point along the line of twofold saturation which, in turn, permits calculation of the volume fractions of each eutectic-type constituent present in the as-solidified microstructure. These relations are derived assuming that Nb and C each exhibit negligible diffusion in the austenite matrix. While this is a good assumption for Nb [7], the opposite extreme of infinitely fast diffusion is more appropriate for C [7, 10]. The M–F model is modified below to allow for such behavior.

3.2. Negligible Nb diffusion/infinately fast C diffusion

The relation describing the variation in Nb and C contents in the liquid during primary γ solidification under conditions of negligible Nb diffusion and infinitely fast C diffusion can be obtained in the same manner used to derive equation (1), except the Scheil equation is replaced by the equilibrium lever law to provide the relation between fraction liquid and liquid composition for carbon

$$f_l = \frac{C_{o,C} - k_c C_{1,C}}{(1 - k_c) C_{1,C}}. \quad (13a)$$

The f_l – C_l relation for Nb is still given through the Scheil equation

$$f_l = \left(\frac{C_{1,Nb}}{C_{o,Nb}} \right)^{1/(k_{Nb}-1)}. \quad (13b)$$

Proceeding in the same manner used by Mehrabian and Flemings to derive equation (1), equations (13a)–(b) are equated (since f_l can only have one value) and solved for $C_{1,Nb}$ to obtain a solidification path relation

$$C_{1,Nb} = C_{o,Nb} \left[\frac{C_{o,C} - k_c C_{1,C}}{(1 - k_c) C_{1,C}} \right]^{k_{Nb}-1}. \quad (13c)$$

This relation is analogous to equation (1) of the M–F model. The procedure for calculating the total volume fraction of eutectic-type constituents which form after primary solidification is similar to that described above for the M–F model. The carbon content at the intersection point of the primary solidification path with the line of twofold saturation is given by

$$\frac{C_{1,C} - a}{b} = C_{o,Nb} \left[\frac{C_{o,C} - k_c C_{1,C}}{(1 - k_c) C_{1,C}} \right]^{k_{Nb}-1}. \quad (14)$$

The corresponding Nb content, $C_{1,Nb}$, is calculated by back substitution of this value of $C_{1,C}$ into equation (2) or equation (13c), and this value of $C_{1,Nb}$ is used to calculate the total amount of eutectic-type constituent through equation (4).

Since Nb diffusion is still assumed negligible, the differential mass balance for Nb along the line of twofold saturation as given by equation (8a) in the M–F model remains valid. For C, the equilibrium lever law is used with the addition of a new term to account for formation of NbC from the liquid. The equilibrium mass balance for C along the line of twofold saturation is given by

$$C_{o,C} = f_l C_{1,C} + f_\gamma C_{\gamma,C} + f_{NbC} C_{NbC,C}. \quad (15)$$

Proceeding in the same manner used in the M–F model, equation (15) is joined with

$$f_\gamma = 1 - f_{NbC} - f_l \quad (16)$$

$$C_{\gamma,C} = k_{\gamma,C} C_{1,C} \quad (17)$$

to define a relation between f_{NbC} and $C_{1,Nb}$

$$f_{NbC} = \frac{C_{o,C} - C_{1,C} [f_l + k_{\gamma,C} (1 - f_l)]}{(C_{NbC,C} - k_{\gamma,C} C_{1,C})}. \quad (18)$$

Under the general case of a second phase forming (which, in this particular case, is the NbC phase), the composition of the secondary solid phase would have to be expressed in terms of the liquid composition through the distribution coefficient in order to arrive at a general expression for f_{NbC} in terms of the liquid composition. However, in this particular case, the NbC is a stoichiometric compound which forms at constant composition. Thus, $C_{NbC,C}$ is a constant in equation (18) and such an approach is not needed.

Table 2. Summary of solidification parameters used in calculations

| Quantity | Ni base alloys | Fe base alloys | Units |
|---|----------------|----------------|--------------|
| $k_{\gamma\text{Nb}}$ | 0.45 | 0.25 | unitless |
| $k_{\gamma\text{C}}$ | 0.21 | 0.21 | unitless |
| $C_{\text{NbC,Nb}}$ | 90.5 | 90.5 | wt% Nb |
| $C_{\text{NbC,C}}$ | 9.5 | 9.5 | wt% C |
| a | 1.13 | 1.37 | wt% C |
| b | -0.047 | -0.065 | wt% C/wt% Nb |
| $C_{\text{Nb,L} \rightarrow (\gamma + \text{Laves})}$ | 23.1 | 20.4 | wt% Nb |
| $C_{\text{C,L} \rightarrow (\gamma + \text{Laves})}$ | 0.04 | 0.04 | wt% C |

The expression for $df_{\text{NbC}}/dC_{1,\text{C}}$ is given by

$$\frac{df_{\text{NbC}}}{dC_{1,\text{C}}} = \frac{k_{\gamma,\text{C}}C_{0,\text{C}} - C_{\text{NbC,C}}[f_1 + k_{\gamma,\text{C}}(1-f_1)]}{(C_{\text{NbC,C}} - k_{\gamma,\text{C}}C_{1,\text{C}})^2}. \quad (19)$$

Equation (9) is inserted into equation (19) to arrive at the desired relationship between df_{NbC} and $dC_{1,\text{Nb}}$

$$\frac{df_{\text{NbC}}}{dC_{1,\text{Nb}}} = \frac{bk_{\gamma,\text{C}}C_{0,\text{C}} - bC_{\text{NbC,C}}[f_1 + k_{\gamma,\text{C}}(1-f_1)]}{(C_{\text{NbC,C}} - k_{\gamma,\text{C}}C_{1,\text{C}})^2}. \quad (20)$$

Equation (20) is analogous to equation (10) of the M-F model. Equation (20) is inserted into equation (8a) to obtain the final relation between df_1 and $dC_{1,\text{Nb}}$

$$\frac{df_1}{dC_{1,\text{Nb}}} = -\frac{1}{(1-k_{\gamma,\text{Nb}})C_{1,\text{Nb}}} - \left[\frac{(k_{\text{NbC,Nb}} - k_{\gamma,\text{Nb}})}{(1-k_{\gamma,\text{Nb}})} \right] \left[\frac{bk_{\gamma,\text{C}}C_{0,\text{C}} - bC_{\text{NbC,C}}[f_1 + k_{\gamma,\text{C}}(1-f_1)]}{(C_{\text{NbC,C}} - k_{\gamma,\text{C}}C_{1,\text{C}})^2} \right]. \quad (21)$$

Equation (21) is analogous to equation (11) in the M-F model, and the calculation procedure is conducted in the same manner described previously. These relations are utilized in the next section to

calculate the total and individual amounts of eutectic type constituents which form in the experimental alloys.

4. RESULTS AND DISCUSSION

The parameters used to calculate the compositions and fractions of each phase forming during solidification were previously determined [1, 6, 7] and are summarized in Table 2. The values of $C_{\text{Nb,L} \rightarrow (\gamma + \text{Laves})}$ and $C_{\text{C,L} \rightarrow (\gamma + \text{Laves})}$ listed in Table 2 represent the point of the class II reaction on the solidification surfaces where the $\text{L} \rightarrow (\gamma + \text{NbC})$ reaction is replaced by the $\text{L} \rightarrow (\gamma + \text{Laves})$ reaction. When the Nb and C contents in the liquid reach these points, the remaining liquid (f_1) transforms to the γ/Laves constituent ($f_{\gamma/\text{Laves}}$) and the calculations are terminated. The amount of the γ/NbC constituent is then given by $f_{\gamma/\text{NbC}} = f_e - f_{\gamma/\text{Laves}}$, where f_e is the total amount of eutectic-type constituent. The value of f_e is calculated by determining the fraction of liquid remaining at the point where the primary solidification path intersects the line of twofold saturation. The constants a and b were determined by linear regression analysis from the point of

Table 3. Phase identification summary and quantitative image analysis results

| Alloy | Phases present | Total eutectic-type constituent (vol.%) | γ/NbC (vol.%) | γ/Laves (vol.%) |
|-------|----------------|---|-----------------------------|-------------------------------|
| 1 | ? | 0.8 ± 0.2 | — | — |
| 1.5 | NbC† | 1.6 ± 0.4 | — | — |
| 2 | NbC | 5.2 ± 1.5 | 5.2 ± 1.5 | 0 |
| 3 | NbC, Laves | 1.2 ± 0.7 | — | — |
| 3.5 | NbC | 3.0 ± 0.4 | 3.0 ± 0.4 | 0 |
| 4 | NbC | 7.3 ± 1.3 | 7.3 ± 1.3 | 0 |
| 5 | NbC, Laves | 2.5 ± 1.1 | $\sim 0\ddagger$ | $\sim 2.5 \pm 1.1$ |
| 6 | NbC, Laves | 13.3 ± 2.5 | $\sim 13.3 \pm 2.5$ | $\sim 0\ddagger$ |
| 7 | NbC, Laves | 2.7 ± 0.4 | $\sim 0\ddagger$ | $\sim 2.7 \pm 0.4$ |
| 7.5 | NbC, Laves | 7.5 ± 0.5 | 5.2 ± 0.5 | 2.3 ± 0.5 |
| 8 | NbC, Laves | 15.2 ± 1.6 | 13.7 ± 1.6 | 1.5 ± 0.7 |
| 9 | NbC, Laves | 3.8 ± 0.5 | $\sim 0\ddagger$ | $\sim 3.8 \pm 0.5$ |
| 10 | NbC, Laves | 9.0 ± 1.0 | $\sim 9.0 \pm 1.0$ | $\sim 0\ddagger$ |
| 11 | NbC, Laves | 2.5 ± 0.4 | $\sim 0\ddagger$ | $\sim 2.5 \pm 0.4$ |
| 11.5 | NbC, Laves | 7.3 ± 1.1 | 6.6 ± 1.1 | 0.7 ± 0.1 |
| 12 | NbC, Laves | 6.7 ± 1.7 | 4.4 ± 1.7 | 2.3 ± 0.8 |
| 13 | NbC, Laves | 12.9 ± 1.4 | $\sim 0\ddagger$ | $\sim 12.9 \pm 1.4$ |
| 14 | NbC, Laves | 23.8 ± 1.6 | 18.8 ± 1.6 | 5.0 ± 0.6 |
| 15 | NbC, Laves | 15.5 ± 1.4 | $\sim 0\ddagger$ | 15.5 ± 1.4 |
| 16 | NbC, Laves | 23.6 ± 2.1 | 17.5 ± 2.1 | 6.1 ± 0.7 |

†May contain Laves also.

‡Contains trace amounts of γ/NbC .

§Contains trace amounts γ/Laves .

Table 4. Summary of secondary solidification reaction temperatures

| Alloy | L \rightarrow (γ + NbC) reaction start temp. (°C) | L \rightarrow (γ + Laves) reaction start temp. (°C) |
|-------|---|---|
| 2 | 1341.5 \pm 0.7 | — |
| 3.5 | 1322 \pm 1.4 | — |
| 4 | 1330.0 \pm 1.3 | — |
| 6 | 1332.0 \pm 1.4 | ND |
| 7.5 | 1305.5 \pm 0.7 | ND |
| 8 | 1328.0 \pm 2.8 | ND |
| Ni-1 | — | 1190 |
| 10 | 1357.5 \pm 0.7 | ND |
| 11.5 | 1347.5 \pm 2.1 | ND |
| 12 | 1348.0 \pm 1.4 | ND |
| 13 | 1332.5 \pm 0.7 | 1249.5 \pm 3.5 |
| 14 | 1360.8 \pm 2.2 | 1243.0 \pm 2.1 |
| 15 | 1289.5 \pm 0.8 | 1256.3 \pm 1.2 |
| 16 | 1355.2 \pm 1.7 | 1248.2 \pm 4.8 |
| Fe-1 | 1325 | 1266 |

ND, not detected.

($C_{Nb,L \rightarrow (\gamma + Laves)}$, $C_{C,L \rightarrow (\gamma + Laves)}$) to the data points on the line of twofold saturation separating the γ and NbC phases. The measured volume fractions of eutectic constituents in each alloy are sum-

marized in Table 3 and the reaction temperatures for the L \rightarrow (γ + NbC) and L \rightarrow (γ + Laves) reactions are listed in Table 4.

4.1. Primary L \rightarrow γ solidification

The primary solidification path of each alloy was calculated via equation (13c) (Nb diffusion negligible and C diffusion infinitely fast) and plotted on the respective solidification surface. The results of the calculations are presented in Figs 1, 2 and 3. Figures 1 and 2 plot the results for the Ni base and Fe base alloys, respectively. The results are grouped according to alloys with similar Nb contents. Figure 3(a) compares the solidification paths of Ni base alloys with similar C contents and variations in Nb, and Fig. 3(b) compares the solidification paths of a Ni base and Fe base alloy with similar levels of solute elements. The alloy number associated with each solidification path is noted in the figures. The solidification path for each alloy initiates at the nominal composition and progresses

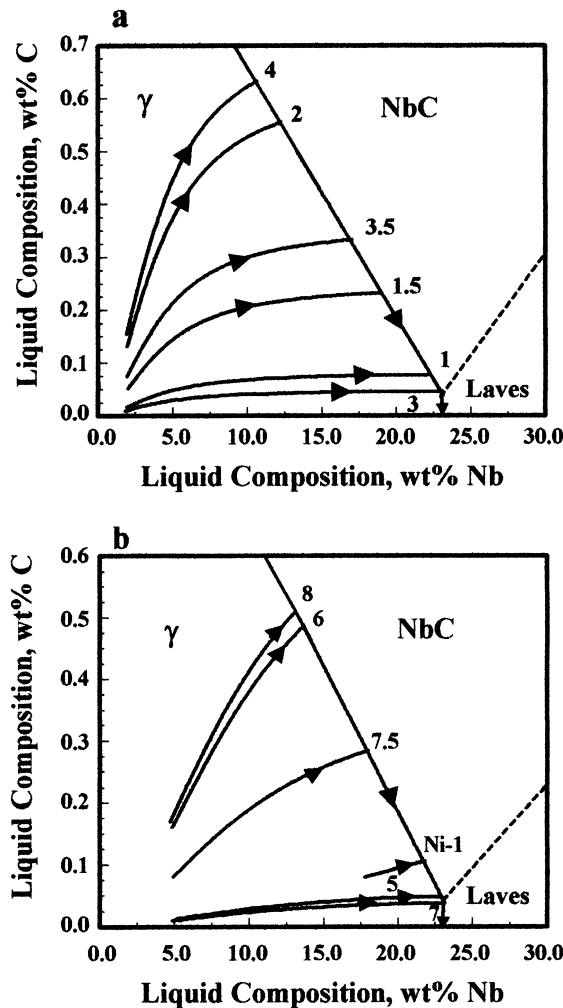


Fig. 1. Calculated solidification paths for the Ni base alloys: (a) low Nb alloys; (b) high Nb alloys.

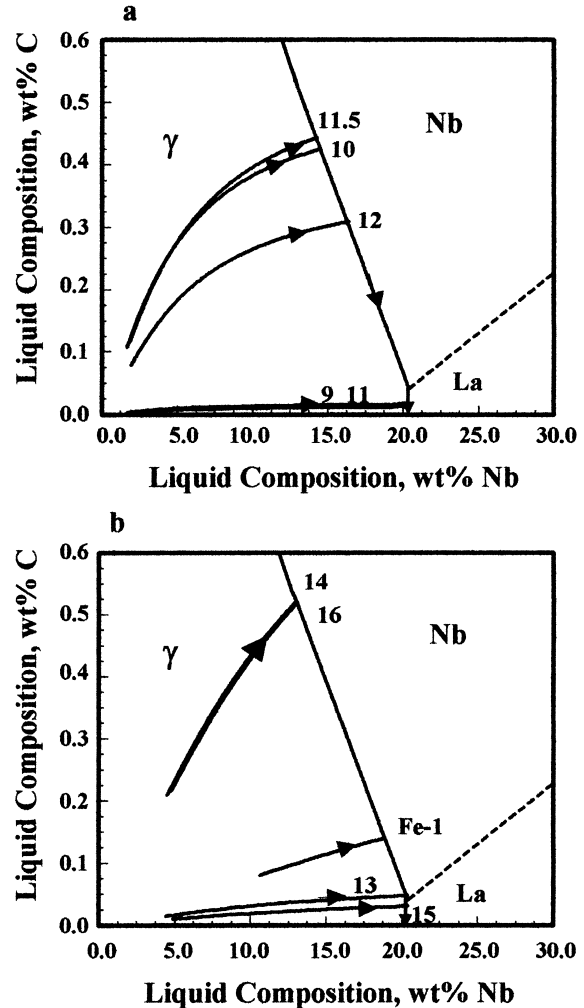


Fig. 2. Calculated solidification paths for the Fe base alloys: (a) low Nb alloys; (b) high Nb alloys.

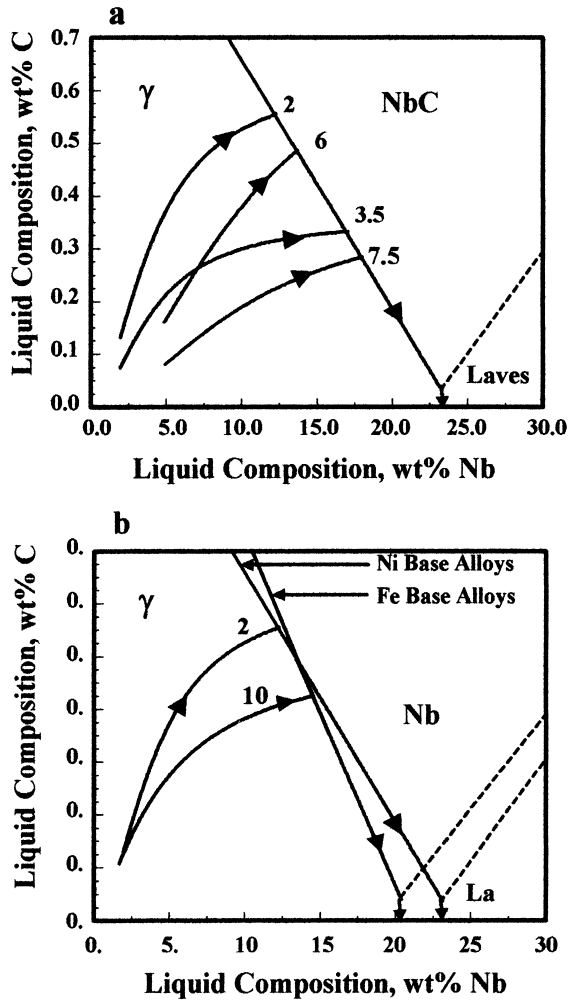


Fig. 3. (a) Calculated solidification paths of Alloys 2, 3.5, 6, and 7.5. (b) Calculated solidification paths of Alloys 2 and 10.

toward the line of twofold saturation between γ and NbC as the liquid becomes enriched in Nb and C. When the primary $L \rightarrow \gamma$ path strikes the line of twofold saturation, solidification then proceeds along the line of twofold saturation in the direction of decreasing temperature (i.e. toward the γ -Nb “binary”). The amount of solid formed during primary solidification is proportional to the total distance of the primary solidification path. This relation is useful as it allows for qualitative interpretations of alloying effects by simple visual inspection of the results.

These calculations illustrate several key features concerning the solidification behavior of these alloys. First, it is readily apparent that the point of intersection between the primary solidification path and line of twofold saturation is a strong function of C content. Although C additions are intuitively expected to promote the γ /NbC eutectic type constituent, this analysis provides a quantitative rationale for the observed behavior. The intersection

point occurs at higher C contents as the nominal C content of the alloy increases. As a result, the liquid composition must “travel” a long distance down the $L \rightarrow (\gamma + \text{NbC})$ line of twofold saturation, forming γ /NbC as it travels, before the γ /Laves constituent can possibly form. The relative temperature at which the $L \rightarrow (\gamma + \text{NbC})$ reaction starts is also readily assessed, where high nominal C contents drive the initiation of the reaction to higher temperatures. The experimental DTA data generally show this trend (e.g. compare Alloy 3.5 to 4 and Alloy 7.5 to 8 in Table 4). The only exception to this behavior occurs between alloys with variations in Si content. For example, Fig. 1(b) suggests that Alloy 8 should have a higher reaction start temperature than Alloy 6, but the experimental DTA data reveals the opposite case. This difference is caused by the higher Si content of Alloy 8. Since the liquidus slope for Si is negative [1], the liquidus surface for Alloy 8 is shifted to a lower temperature relative to the surface of Alloy 6. As shown previously [6], the Si content of the γ /NbC constituent in Alloy 8 is higher than that of Alloy 6 and supports this. This pseudo-ternary approach cannot account for such effects from a third solute element. However, the general influence of Si will become apparent in the modeling results and will be discussed in qualitative terms where appropriate.

The increase in reaction temperature with increasing C content is not initially intuitive, particularly when one considers that the liquidus slope for C is negative [1]. This, at first, suggests that any increase in carbon in the liquid should drive the reaction to lower temperatures. The true effect can be understood by considering the relation between Nb and C along the line of twofold saturation. The slope of this line, **b**, is $-0.047 \text{ wt\% C/wt\% Nb}$ for the Ni base alloys. Thus, for every 0.047 wt% increase in C content, there is a corresponding decrease of 1 wt% Nb in the liquid. Assuming the liquidus slope for each element is constant and equal to the values determined by Cieslak *et al.* [1]: $m_{1,C} = -108.6^\circ\text{C/wt\% C}$ and $m_{1,Nb} = -11.1^\circ\text{C/wt\% Nb}$, then there is a drop in the reaction temperature of $\approx 5.1^\circ\text{C}$ for every increase of 0.047 wt% C and a simultaneous increase in the reaction temperature of 11.1°C for the corresponding decrease in 1 wt% Nb content. Thus, a net increase of 6°C in reaction temperature is expected with every 0.047 wt% increase in C content (1 wt% decrease in Nb content). This effect causes the reaction start temperature to increase with increasing nominal carbon content.

The effect of nominal Nb concentration is revealed by comparing Alloy 2 to 6 and Alloy 3.5 to 7.5 in Fig. 3(a). When Nb is low, the C content in the liquid increases relatively quickly during the early stage of solidification. The rate of C enrichment continuously decreases as the line of twofold saturation is approached. Overall, the reaction start

temperature will increase with decreasing Nb (i.e. increasing C/Nb ratio). Again, this trend is consistent with the experimental DTA data. Since the length of the primary solidification paths for the high Nb alloys are shorter, these alloys will exhibit more liquid at the intersection point (i.e. more total eutectic-type constituent). The primary solidification paths of the two high Nb alloys (Ni-1 and Fe-1) are also plotted. The primary solidification path intersects the γ /NbC twofold saturation line just above the class II reaction point. At this stage, there is a large fraction of liquid which is high in Nb. Each alloy then forms a large amount of the γ /Laves constituent after traveling a relatively short distance down the $L \rightarrow (\gamma + \text{NbC})$ reaction line. The nominal composition of Alloy Ni-1 is particularly close to the $L \rightarrow (\gamma + \text{NbC})$ reaction line. This may account for the previous difficulty encountered in revealing two distinct reaction peaks in the DTA scan [6].

The effect of matrix composition is presented in Fig. 3(b). Alloys 2 and 10 have very similar levels of solute content, but different matrix compositions. The main difference here is in the value of k_{Nb} (k_{Nb} in Ni base alloys equals 0.45 while k_{Nb} in the Fe base alloys equals 0.25). As k is reduced, Nb segregates more aggressively to the liquid. At any given level of C in the liquid, the Fe base alloys will always possess more Nb. As a result, the Fe base alloys will have more liquid remaining after primary solidification, and the Nb content in that remaining liquid will be higher. These two effects from the reduced k_{Nb} value, combined with the slightly lower $L \rightarrow (\gamma + \text{Laves})$ "eutectic" composition of (20.4 wt% Nb for the Fe base alloys vs 23.1 wt% Nb for the Ni base alloys), are the reasons for the higher amounts of total and γ /Laves eutectic-type constituents observed in the Fe base alloys.

Lastly, the order of eutectic-type reactions predicted by this approach is readily read from the diagrams. Any alloy which exhibits a primary $L \rightarrow \gamma$ path that terminates above the class II reaction is expected to undergo the $L \rightarrow (\gamma + \text{NbC})$ reaction prior to terminating solidification with the $L \rightarrow (\gamma + \text{Laves})$ reaction. This behavior is predicted for all the alloys except 7, 9, 11, and 15. This is in reasonable agreement with experimental observations, where all the alloys exhibited the NbC phase. The point of the class II reaction is taken from an average of all the Nb values determined in the γ /Laves constituent. However, this point is actually dependent on the amount of Fe, Cr, and Si in the liquid [6, 7]. The Nb content in the liquid required to satisfy the condition for the $L \rightarrow (\gamma + \text{Laves})$ reaction generally decreases with increasing Fe, Cr, and Si. Thus, representing the class II reaction as a single point will lead to some error and is likely responsible for the discrepancy observed.

The accuracy of this pseudo-ternary approach for the primary $L \rightarrow \gamma$ reaction portion of solidification can be evaluated by comparing the values of calculated and measured amounts of total eutectic-type constituent. In order to maintain consistency of units, the measured volume percent of the γ /NbC and γ /Laves constituents should strictly be expressed in weight fractions. However, it has been shown that the densities of the γ , NbC, and Laves phases are very similar [2]. Thus, the use of volume fractions can be used with introduction of little error. The results of the comparison are plotted in Fig. 4. The correlation between calculated and measured total eutectic constituent is reasonable, especially considering that the input data for this model comes from a number of different experimental techniques (EPMA, QIA, wet chemical analysis).

4.2. Eutectic-type solidification

Solute redistribution during the eutectic-type solidification stage was calculated for each alloy using equation (21). Figure 5(a) shows a typical calculation result for the entire solidification process (for Alloy 4), and the final stages of solidification are shown in more detail in Fig. 5(b). For the final eutectic-type stages of solidification, comparison is made between the behavior predicted by the M-F model and the modified form of the M-F model applied in this work. For clarity, the comparison is made assuming that the fraction liquid existing at the start of the $L \rightarrow (\gamma + \text{NbC})$ reaction is equivalent for the two models. (Note, however, that the M-F model for the primary $L \rightarrow \gamma$ stage of solidification would predict a different (higher) value of fraction liquid at the start of the $L \rightarrow (\gamma + \text{NbC})$ reaction.) Solute redistribution during the $L \rightarrow (\gamma + \text{NbC})$ reaction was calculated until solidi-

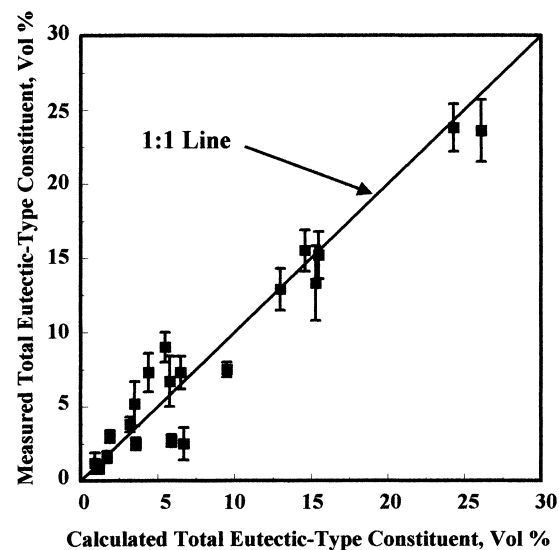


Fig. 4. Comparison between calculated and measured total volume percentages of eutectic-type constituents.

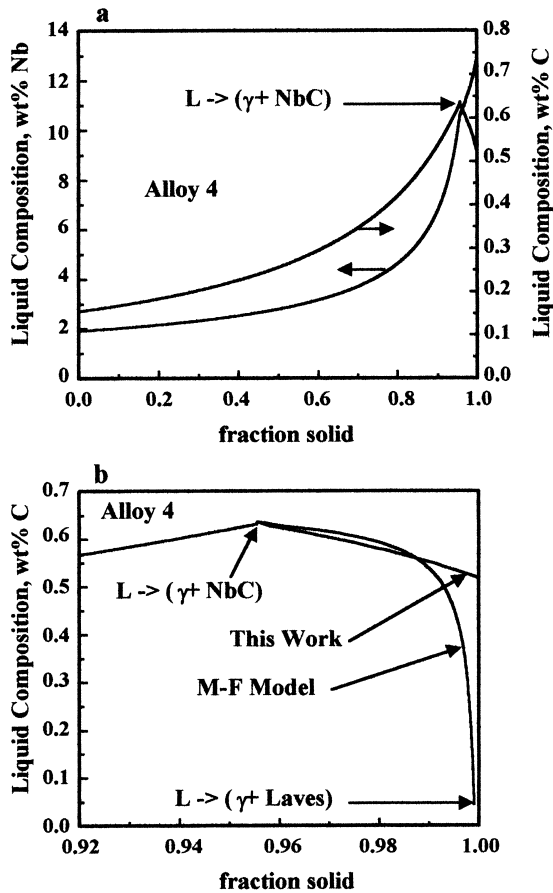


Fig. 5. (a) Calculated variation in Nb and C content in liquid as a function of fraction solid in Alloy 4 for the entire solidification process. (b) Calculated variation in C content in the liquid for Alloy 4 during the final stages of solidification.

fication was either complete ($f_l=0$) or the liquid composition became enriched in Nb and depleted in C to the point where the $L \rightarrow (\gamma + Laves)$ reaction was initiated. At this point, the remaining liquid transforms to the $\gamma/Laves$ constituent and the calculations were terminated. For the case shown, the results predict that the $L \rightarrow (\gamma + NbC)$ reaction is initiated when the fraction liquid is 0.044. The M-F model shows that a small amount of the $\gamma/Laves$ constituent will form at the end of solidification. When the M-F model is modified to account for the high diffusivity of C in the solid, solidification is predicted to be complete before the liquid satisfies the composition requirements for the $L \rightarrow (\gamma + Laves)$ reaction (as was observed experimentally for Alloy 4).

The M-F model was developed under the same assumptions used to derive the Scheil equation and represents the most severe case of microsegregation. Thus, just as in the analogous two-component Scheil equation, this model predicts that some finite amount of liquid will always persist during solidification until it becomes sufficiently rich in solute to

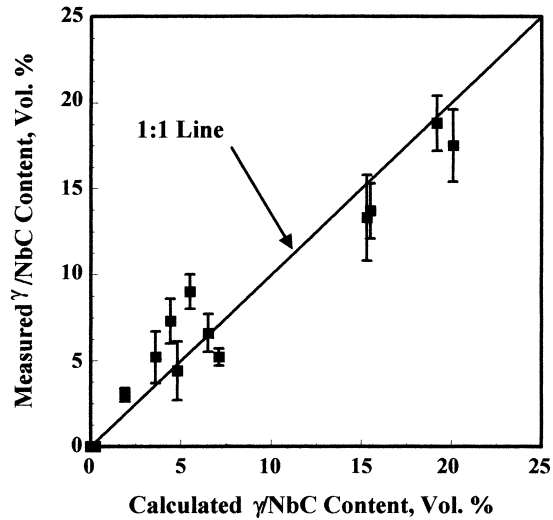


Fig. 6. Comparison between measured and calculated volume percentages of γ/NbC eutectic-type constituent.

reach a local minimum on the liquidus surface. At this point, solidification will terminate via the appropriate reaction which exists at the local minimum. For the particular alloys studied here, this implies that some finite amount of the $\gamma/Laves$ constituent will always be predicted by the M-F model. Any departure of this condition towards equilibrium behavior, which occurs when C is allowed to diffuse infinitely fast, will modify this extreme condition. As a result of this effect, it is possible for solidification to be completed along the $L \rightarrow (\gamma + NbC)$ reaction line before the liquid composition has a chance to satisfy conditions for the $L \rightarrow (\gamma + Laves)$ reaction. This solidification sequence is predicted for Alloys 1.5, 2, 3.5, 4, 6, 8, 10, and 11.5. Experimentally, this solidification sequence was observed in Alloys 2, 3.5, and 4.

The measured and calculated values of the individual eutectic-type constituents are compared in Figs 6 and 7. The modified form does accurately predict the completion of solidification during the $L \rightarrow (\gamma + NbC)$ reaction for Alloys 2, 3.5, and 4, as no $\gamma/Laves$ constituent was observed in these alloys. However, the model also predicts that no $\gamma/Laves$ should be present in Alloys 6, 8, 10, and 11.5, while this constituent is observed experimentally in small amounts. Considering the assumptions invoked with this approach, the resolution of such fine detail is not expected. The presence of $\gamma/Laves$ in Alloys 8 and 11.5 can be attributed to their high Si content, since less Nb is needed in the liquid to satisfy conditions for the $L \rightarrow (\gamma + Laves)$ reaction as the Si content is raised. For a given alloy, the Si content in the γ/NbC constituent is always lower than that in the $\gamma/Laves$ [6]. This indicates that the distribution coefficient for Si remains below unity during the $L \rightarrow (\gamma + NbC)$ reaction. Thus, the line of two-fold saturation for the $L \rightarrow (\gamma + NbC)$ reaction is actually shifting to lower Nb values as solidification

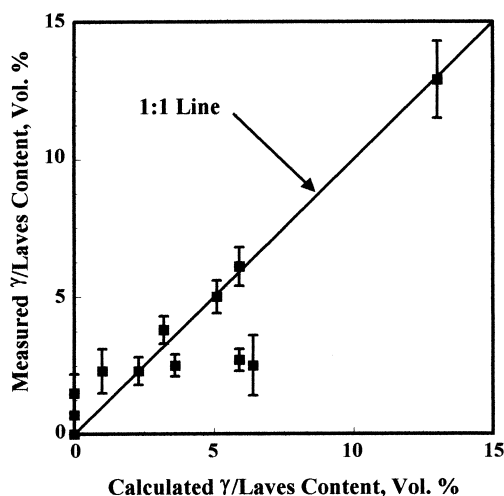


Fig. 7. Comparison between measured and calculated volume percentages of γ /Laves eutectic-type constituent.

progresses. Alloys with higher nominal Si contents will induce more of a shift in the position and are therefore more likely to reach the composition conditions for the $L \rightarrow (\gamma + \text{Laves})$ reaction. All other factors being equal, the higher Si alloys always show the larger amount of γ /Laves (e.g. compare Alloy 6 to 8 and Alloy 10 to 11.5). Such effects from a third solute cannot be accounted for with this pseudo-ternary approach. Nevertheless, there is reasonable agreement between measured and calculated total and individual eutectic-type constituents. This confirms that the model developed here correctly captures the major factors controlling the solidification behavior of this class of alloys. In addition, the modified form of the M-F model developed here is general enough to apply to other alloy systems in which variations in the diffusion behavior of one of the solutes may lead to more pronounced effects.

5. SUMMARY

Solute redistribution and microstructural evolution have been modeled for experimental Nb-bearing superalloys. The multi-component alloys were modeled as a ternary system by grouping the matrix (Fe, Ni, Cr) elements together as the "solvent" to form the γ component of the γ -Nb-C "ternary system". Solute redistribution equations for solidification of a ternary alloy were proposed for conditions in which one solute exhibits negligible diffusion in the solid phase while the other solute diffuses fast enough to maintain equilibrium. The model was applied to calculate the variation in fraction liquid

and liquid composition during the primary $L \rightarrow \gamma$ and eutectic type $L \rightarrow (\gamma + \text{NbC})$ stages of solidification for the γ -Nb-C system of interest. Comparison is made to experimentally measured values, and reasonable agreement was found. Carbon additions were found to have a pronounced effect on microstructural development by controlling the primary solidification path. As the C content in the alloy is increased, the primary $L \rightarrow \gamma$ solidification path extends far into the C rich side of the solidification surface as the interdendritic liquid becomes enriched in C. This primary path orientation favors the $L \rightarrow (\gamma + \text{NbC})$ eutectic type reaction, and large amounts of the γ /NbC eutectic type constituent form as a result. In contrast, low C alloys exhibit a primary solidification path which remains close to the "binary" γ -Nb edge of the solidification surface where the $L \rightarrow (\gamma + \text{Laves})$ eutectic type reaction is favored. The segregation potential of Nb is higher in Fe base alloys ($k_{\text{Nb}} = 0.25$) than in Ni base alloys ($k_{\text{Nb}} = 0.45$). This difference causes more solute rich interdendritic liquid to be present in the Fe base alloys when the eutectic type reactions are initiated which, in turn, produces more of the eutectic-type constituents in the as-solidified microstructure.

Acknowledgements—One author (J.N.D.) gratefully acknowledges financial support for this research from the American Welding Society Fellowship Award. Sandia is a multi-program laboratory operated by Sandia Corporation, a Lockheed Martin Company, for the United States Department of Energy under Contract DE-AC04-94AL85000.

REFERENCES

1. Cieslak, M. J., Headley, T. J., Kollie, T. and Romig, A. D., *Metall. Trans.*, 1988, **19A**, 2319.
2. Knorovsky, G. A., Cieslak, M. J., Headley, T. J., Romig, A. D. and Hammett, W. F., *Metall. Trans.*, 1989, **20A**, 2149.
3. Nakkalil, R., Richards, N. L. and Chturvedi, M. C., *Metall. Trans.*, 1993, **24A**, 1169.
4. Cieslak, M. J., Headley, T. J., Knorovsky, G. A., Romig, A. D. and Kollie, T., *Metall. Trans.*, 1990, **21A**, 479.
5. Robino, C. V., Michael, J. R. and Cieslak, M. J., *Sci. Technol. Welding Joining*, 1997, **2**, 220.
6. DuPont, J. N., Robino, C. V., Marder, A. R., Notis, M. R. and Michael, J. R., *Metall. Trans.*, in press.
7. DuPont, J. N., Robino, C. V., Marder, A. R. and Notis, M. R., *Metall. Trans.*, in press.
8. Mehrabian, R. and Flemings, M. C., *Metall. Trans.*, 1970, **1**, 455.
9. Kajihara, M., Yoshikawa, T., Kikuchi, M. and Yamauchi, K., *Iron Steel Inst. Japan*, 1992, **32**, 755.
10. Clyne, T. W. and Kurz, W., *Metall. Trans.*, 1981, **12A**, 965.